This is the accepted manuscript version (post-print) of the work that was accepted for publication in the ASME Journal of Engineering for Gas Turbines and Power published online, December 2022.

The final version was published as:
Meier zu Ummeln, R., Moreau, A., and Schnoes, M. (2022). Influence of Different Flow Solvers and Off-Design Conditions On the Determination of Fan-Rotor Wakes for Broadband Noise Prediction. *Journal of Engineering for Gas Turbines and Power*, GTP-22-1471, 145(3), March 2023.
https://doi.org/10.1115/1.4055753

Influence of different flow solvers and off-design conditions on the determination of fan-rotor wakes for broadband noise prediction

Robert Meier zu Ummeln
German Aerospace Center (DLR)
Institute of Propulsion Technology
10623 Berlin, Germany
Email: robert.meierzuummeln@dlr.de

Antoine Moreau
German Aerospace Center (DLR)
Institute of Propulsion Technology
10623 Berlin, Germany
Email: antoine.moreau@dlr.de

Markus Schnoes
German Aerospace Center (DLR)
Institute of Propulsion Technology
51147 Cologne, Germany
Email: markus.schnoes@dlr.de

ABSTRACT

The acoustic interaction of fan-rotor wakes with the downstream stator vanes is considered as an important noise source of an aircraft engine. The turbulence induced by the rotor generates a stochastic acoustic source that appears as broadband noise in the acoustic spectrum. During the preliminary design phase of an engine, established meanline and throughflow solvers usually do not resolve turbulence and associated unsteady flow parameters. But such solvers provide rotor pressure losses that can be used to estimate the mean and turbulent rotor wakes. A crucial step is the

deduction of turbulence parameters from the mean wakes. A semi-empirical model for rotor-wake turbulence estimation is presented in this paper. The meanline method and the throughflow solver are compared to three-dimensional computational flow simulations investigating the capabilities of the different solvers to provide flow data for broadband wake interaction noise prediction. The methods are applied to a representative modern fan stage at a comprehensive number of operating points, comprising several speed lines from surge to choking conditions. Microphone measurements are consulted to assess the noise predictions. The evaluation confirms the applicability of the meanline and throughflow method in combination with the turbulence model for broadband noise estimation during the preliminary design phase. The underestimated turbulence in the tip region of the fan is found to be negligible even during off-design conditions.

NOMENCLATURE

A $= \int_0^s (v(y)/\overline{W})(\mathrm{d}y/s)$, normalized wake area $[-]$

c profile chord length $[m]$

h wake harmonic order $[-]$

I $= \sqrt{(2/3)k}/W$, turbulent intensity $[-]$

k turbulent kinetic energy (TKE) $[m^2/s^2]$

K calibration factors $[-]$

L $= \Lambda/c$, normalized turbulent integral length scale $[-]$

N rotational fan speed $[\mathrm{min}^{-1}]$

P sound power $[kg \cdot m^2/s^3]$

Q_A mass flow density $[kg/(m^2 s)]$

r radial position $[m]$

Re REYNOLDS number $[-]$

s blade pitch $[m]$

v streamwise velocity perturbation $[m/s]$

w $= AW/v_{\mathrm{max}}$, normalized wake width $[-]$

W streamwise flow velocity $[m/s]$

x axial position $[m]$

y $= r\theta$, circumferential position $[m]$

β flow angle [deg]

θ circumferential angle [deg]

Λ turbulent integral length scale (TLS) $[m]$

ξ off-design loss correction factor $[-]$

Π $= p_{t2}/p_{t1}$, fan pressure ratio $[-]$

ρ density $[kg/m^3]$

ω $= (p_{t1} - p_{t2})_{\mathrm{rel}}/(p_{t1,\mathrm{rel}} - p_1)$, loss coefficient $[-]$

1 INTRODUCTION

The performance, aerodynamics and acoustics are essential disciplines to assess an aircraft engine during the preliminary design phase. Concerning acoustics, the so-called fan rotor-stator wake interaction (RSI) noise source is considered to be an important contributor to the overall noise signature of future aircraft propulsion systems [1–4]. It is essential to find efficient ways to predict this noise source during the preliminary design. Fast, robust, physics-based and comprehensible methods are required during this phase to conduct multidisciplinary optimizations and to explore large parameter spaces. Methods based on analytical formulations satisfy these requirements.

In a previous publication [5], three hybrid approaches were presented that enable to calculate the aerodynamics of the engine's turbofan stage and eventually estimate the aeroacoustic characteristics. For these three approaches, the prediction of the fan acoustics is always based on an analytical method implemented in the DLR (Deutsches Zentrum für Luft- und Raumfahrt, engl. German Aerospace Center) tool PropNoise [6]. As shown in Fig. 1, the approaches differ in the way how the flow is calculated: A 1D meanline approach, hereinafter called *method 1*, calculates the steady flow parameters at a representative radial position in the fan duct and uses an empirical model, briefly described in the *Theory* section, to estimate the turbulence induced by a fan rotor. A 2D throughflow approach, hereinafter called *method 2*, calculates the steady flow on several streamlines distributed in spanwise direction in which the radial equilibrium equation is considered. The same empirical turbulence model, as used for method 1, is applied to each of these streamlines

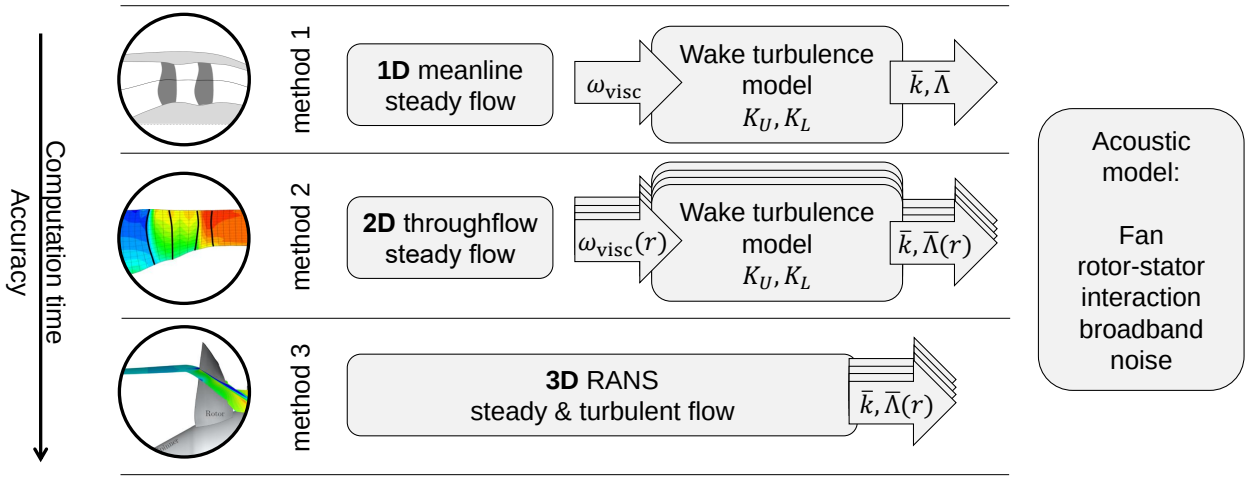

Fig. 1. Investigated hybrid approaches for the prediction of wake-induced fan broadband noise

to calculate the turbulent quantities. Both approaches are very fast, taking about a second on a conventional computer, and they are established approaches for the preliminary design. For a third, RANS-informed (REYNOLDS Averaged NAVIER-STOKES) approach, hereinafter called *method 3*, a numerical simulation of the fan domain is conducted. This approach is time-consuming but it provides detailed insights into the three-dimensional steady flow field as well as turbulence. An extensive comparison of RANS-informed analytical fan broadband noise prediction is given in [7, 8] for the fan investigated in this paper. The predictions show a good agreement with the measurements. LEWIS et al. [9] performed a comparison between RANS-informed and high-fidelity LES-informed (Large-Eddy Simulation) analytical broadband noise prediction which did not yield a remarkable increase in accuracy. Therefore, it can be assumed that a RANS-informed analytical approach is suited to validate the results of the first two, simpler approaches.

The three approaches were applied for a few operating points to four different fan stages in the aforementioned paper [5] and the influence of the turbulence model on broadband RSI noise was investigated. Additionally, the influence of endwall flow on the emitted noise compared to the flow away from the endwalls was quantified. In contrast, in this paper we focus on only one transonic fan stage but extend the number of operating points to a full fan map. It is crucial to understand the differences of the three flow solvers and their effect on the turbulence estimation. By doing so, the influence of flow effects at off-design conditions on the fan broadband noise prediction is investigated. Eventually, the contribution of turbulence produced in the tip region is again evaluated.

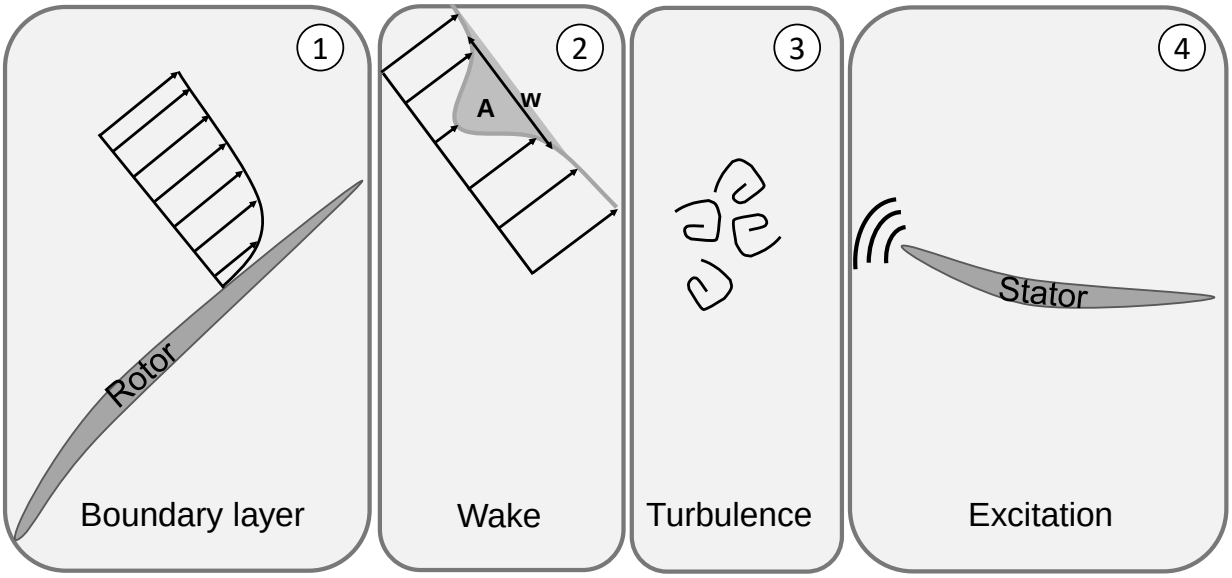

Fig. 2. Radial cut sketch of a rotor-stator fan stage. The rotor blade creates a wake and turbulence which excite the stator blade.

2 THEORY

The turbulent velocity fluctuations induced by the rotor of a fan stage are the source for the broadband component of the RSI noise. In this section, a model for turbulence estimation in rotor wakes is presented.

2.1 Modeling of rotor wakes for broadband noise prediction

The aforementioned methods 1 and 2 do not resolve unsteady flow parameters like turbulence. Instead, they provide steady aerodynamic quantities like mean flow velocities at the leading and trailing edge of blade rows as well as total-pressure losses caused by the blade rows. Figure 2 sketches four steps of a simple approach that derives turbulence from the steady flow which in turn excites the stator vanes and consequently leads to broadband noise. This procedure is concisely described in this section and the associated formulas are specified in the next three sections.

In a first step, the viscous part of the profile losses, which is provoked by the flow friction on the blade's surface and in some cases by flow separation, is used to compute the boundary layer thickness on the profile. The boundary layers on the pressure and suction side of the profile merge into a wake at the trailing edge. In a second step, this forms a velocity deficit in the circumferential direction. We assume that the displacement thickness at the trailing edge remains constant during the wake convection in the downstream direction and

that the wake exhibits a symmetrical Gaussian shape. Thus, the shape can be described with parameters like width, depth and area of the wake profile. The wake propagates further on with the flow towards the stator. During this process, the wake becomes wider and flatter. Far behind the rotor, the wake unifies with adjacent wakes and decays in the free flow.

In a third step, the turbulence distribution in circumferential direction and in front of the subsequent blade row is assumed to have a Gaussian shape like the mean wake. A proportional correlation between the mean and turbulent wake yields the circumferentially averaged turbulent kinetic energy (TKE) and turbulent integral length scale (TLS). We presume that two empirical proportionality constants for TKE and TLS determination exhibit universal character. That is, they remain constant in radial direction and for varying operating conditions. This presumption was checked in the previous paper [5] and is reviewed in this paper.

The turbulent VON KÁRMÁN velocity spectrum can be reconstructed from the TKE and the TLS under the assumption of isotropic turbulence and small correlation lengths. In the last step, the turbulent component in the wake stochastically excites the stator which results in broadband noise and the velocity deficit periodically excites the stator which results in tonal noise.

2.2 Estimation of viscous total-pressure losses

To estimate the viscous total-pressure loss, the throughflow code uses empirical correlations that have been calibrated against MISES [10] computations as presented in [11]. At first, the viscous total-pressure loss at optimum incidence ω^*_{visc} is computed. It is decomposed as outlined by GRIEB [12]:

$$\omega^*_{\mathrm{visc}} = \left(\omega^*_{\mathrm{p,\,inc}} + \Delta\omega^*_{\mathrm{p}}\right) \cdot \left(\frac{\mathrm{Re}}{10^6}\right)^K \tag{1}$$

with profile losses for incompressible flow $\omega^*_{\mathrm{p,\,inc}}$, additional losses due to compressibility $\Delta\omega^*_{\mathrm{p}}$, and a calibration for REYNOLDS number effects. The throughflow code includes correlations to describe shock losses, but these losses should not be considered for the determination of the wake width. The prediction of the incompressible total-pressure loss $\omega^*_{\mathrm{p,\,inc}}$ is based on the equivalent diffusion factor that has been proposed by LIEBLEIN [13] and it includes modifications by KÖNIG [14].

Finally, the overall viscous loss is computed by including an off-design correction ξ:

$$\omega_{\text{visc}} = \omega^*_{\text{visc}}(1 + \xi) \tag{2}$$

The off-design correction is a function of estimated working range and incidence.

2.3 Mean wake

The term *mean wake* describes the time-independent flow velocity profile $v(y)$ in the relative frame of reference of the rotor. This flow profile in circumferential direction is characterized by a velocity deficit due to the presence of a rotor blade. The quantity can only be delivered by methods that take the circumferential flow into account, like the RANS simulation of method 3. Two exemplary sections of such velocity profiles are shown in Fig. 3 (left). The dark line shows the flow velocity over the circumferential angle θ obtained from a CFD (Computational Fluid Dynamics) simulation at a mean radial position of 70% rotor height. For this wake, it is acceptable to assume a GAUSS shape [15], except for the asymmetry provoked by the different boundary layers on the suction and pressure side of the blade profile. Thus, a fit with the GAUSS function

$$v(y) = v_{\max} \cdot e^{-\pi\left(\frac{y}{w \cdot s}\right)^2} \tag{3}$$

yields the non-dimensional wake parameters area A and width w:

$$A \equiv \int_0^s \frac{v(y)}{\overline{W}} \frac{\mathrm{d}y}{s} \tag{4}$$

$$w \equiv A \frac{W}{v_{\max}} \tag{5}$$

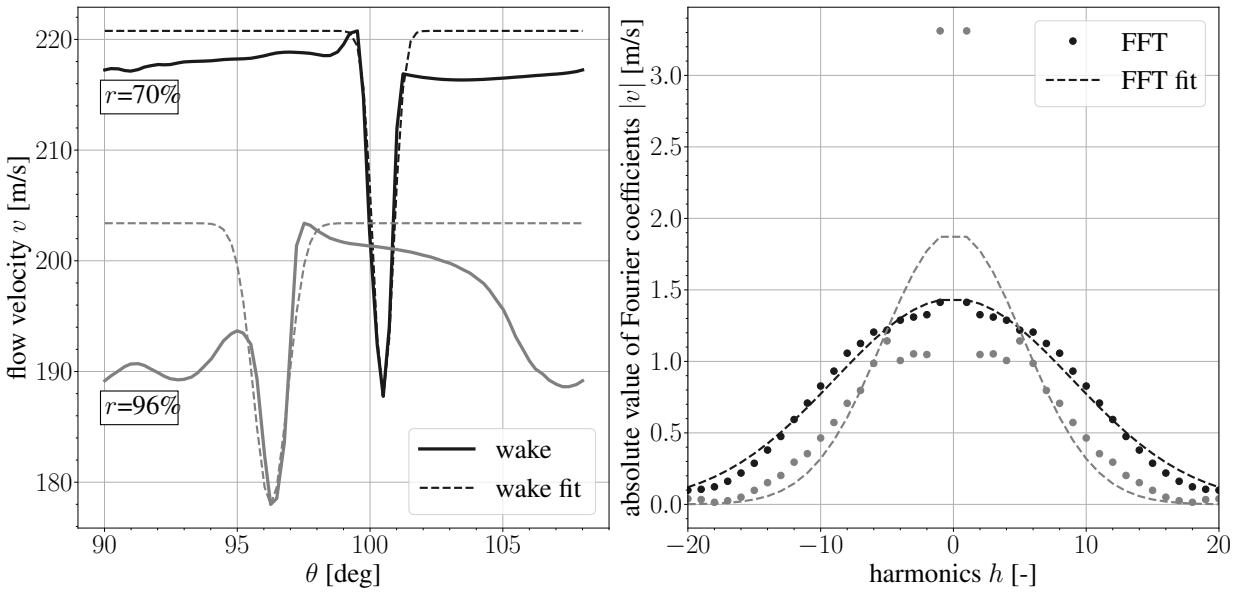

Fig. 3. GAUSS fit of rotor wakes (left) and their FOURIER transforms (right)

with the blade pitch spacing s, the peak perturbation velocity $v_{\max}$, the velocity outside of the wake W and the circumferentially averaged velocity $\overline{W}$.

When approaching the rotor tip area, three-dimensional flow effects alter the shape of the wakes and we start to introduce an increasing error with the GAUSS fit. This becomes apparent when comparing the real wake (solid line) with the wake fit (dashed line) at 96% rotor height in Fig. 3 (left). For this reason, a method to determine the wake parameters in the spatial frequency domain is applied. The analytical solution of the FOURIER transform of Eq. 3 results in another GAUSS function depending on the harmonic order h:

$$v(h) = W \cdot A \cdot e^{-\pi \cdot w^2 \cdot h^2} \tag{6}$$

This function can be fitted with the discrete Fast FOURIER Transform (FFT) of the wakes, shown as dots in Fig. 3 (right). It is challenging to oppose the errors made with the space method to the spatial frequency method. Especially for the lower harmonics an increased error between the FFT and the corresponding fit can be observed. We utilized the coefficient of determination to compare the errors. Additionally, the

radial distribution as well as axial evolution of the wake parameters evaluated from CFD simulations were compared with both methods. It could be observed that the determined wake parameters are much more stable and reliable when obtained from the FFT method.

2.4 Turbulent wake

Several approaches by different authors were introduced in the literature which describe ways to deduce the TLS from mean flow or other turbulence parameters [16–18]. The approach by JURDIC et al. [17] suits the requirements for preliminary design tools since it is based on a simple relationship between the circumferentially averaged TLS $\overline{\Lambda}$ and wake width w:

$$K_L = \frac{\overline{\Lambda}}{w \cdot s \cdot \cos \beta_{\mathrm{rel,out}}} \tag{7}$$

They proposed a proportionality coefficient of $K_L = 0.21$ whereas GANZ et al. [18] indicated values from 0.2 to 0.35 depending on the velocity component.

Another relationship between the circumferentially averaged TKE $\overline{k}$ and the sum of spectral representation of the mean wakes (see Eq. 6) is based on experimental observations made by WYGNANSKI et al. [19].

$$K_U^2 = \frac{\frac{2}{3}\overline{k}}{\sum_h v(h)^2} \tag{8}$$

A value of $K_U = 0.3$ can be deduced from their work.

A RANS-based calibration of those two empirical coefficients was performed in [5] for several fan types at different operating points. The analysis of the RANS-informed turbulence wake interaction noise resulted in values of $K_L = 0.3$ and $K_U = 0.6$. A full description of the turbulence model is also available in that paper.

In order to compare several operating points, these quantities are made non-dimensional as follows:

The TKE is transformed to turbulence intensity $I = \sqrt{(2/3)k}/W$. The TLS is divided by the chord length $L = \Lambda/c$.

3 METHODOLOGY

The meanline and throughflow solver, using the presented turbulence model, and the CFD solver, serving as validation, are applied to a transonic fan stage. All three flow solvers calculate the full fan map of this stage. The fan stage, the flow solvers and the fan map calculation are presented in this section.

3.1 Investigated transonic fan stage

The ACAT1 (AneCom AeroTest Rotor 1) fan stage is a transonic fan with a design pressure ratio of 1.42. It is a scaled 1:3 model compared to the fan stage of a real aircraft engine. The mounted fan stage has a bypass and a core stream with a design bypass ratio of about eight. The fan rotor counts 20 blades. Both the OGV (Outlet Guide Vanes) in the bypass duct and the IGV (Inlet Guide Vanes) in the core duct feature a number of 44 vanes. An extensive database was created in the framework of the EU (European Union) project TurboNoiseBB with the aim to expedite research on the field of broadband noise. For this purpose, experiments were conducted in the Universal Fan Facility (UFFA). The measurements comprise acoustic data by means of pressure sensors [20, 21]. The sound power levels in downstream direction were obtained with 60 wall-flush condenser microphones axially distributed in the bypass duct far behind the OGV. The hydrodynamic and acoustic pressure fluctuations were separated by using an axial wavenumber decomposition method [22]. The sound power levels in upstream direction were measured with 25 far-field microphones which were arranged in a semicircle around the fan inlet. The microphones were located in a large anechoic chamber and the outlet of the bypass and core duct was located outside this chamber. Concerning the broadband noise results, it was assumed by GUÉRIN et al. [8] that spurious noise from other sources than RSI noise was recorded at low frequencies during the experiments.

Several versions of fan geometry and operating points were investigated: The distance between rotor and OGV was varied with a short gap (SG) and a long gap (LG) configuration. Both configurations were investigated at the noise certification operating points *approach*, *sideline* and *cutback*. Additionally, low noise (LN) and sea-level-static (SLS) working lines were explored which differ in blade loading. In this paper, the SG version of the ACAT1 fan is examined. A side view of this configuration is shown in Fig. 4.

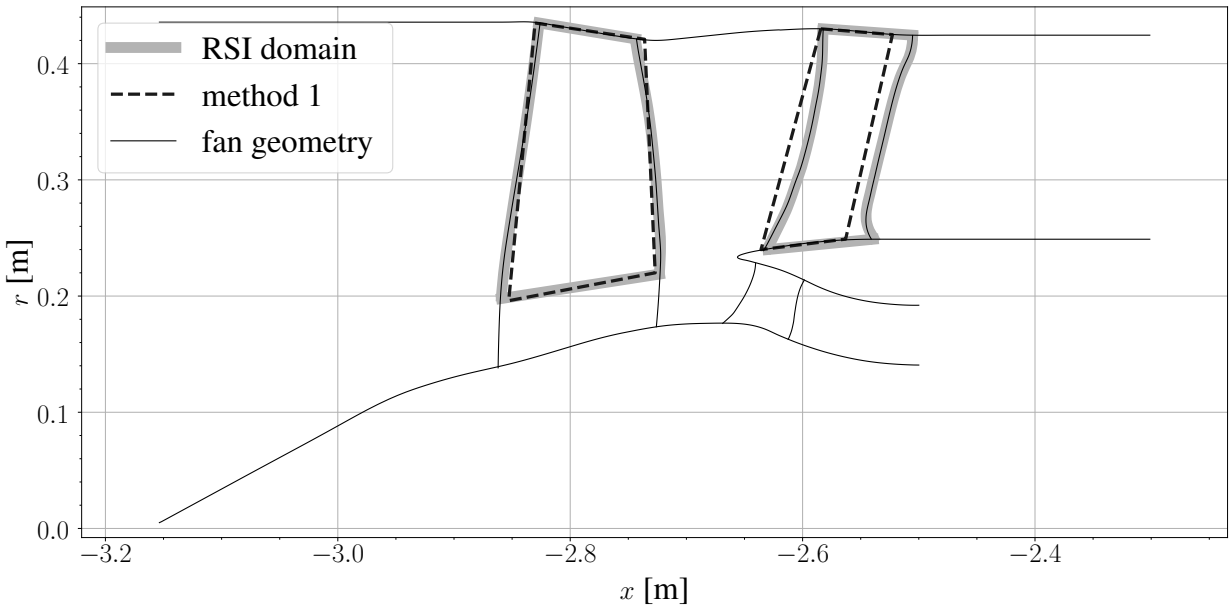

Fig. 4. Meridional cut of the short gap ACAT1 fan stage

The thin black line depicts the original blade geometry and duct contours projected onto the x-r-plane. This geometry is used for the mesh generation of the throughflow and RANS simulation. The projected geometry drawn with thick gray lines describes the domain for the RSI noise calculation. The rotor is truncated in the hub region since only the wake interaction of the rotor with the OGV is considered. Consequently, the flow parameters are only extracted for the mass flow that eventually enters the bypass duct. The determination of the bypass mass flow regime is conducted for every operating point since the streamline dividing core and bypass is expected to move depending on the boundary conditions. The geometry used for the meanline method is a simplified representation of the trimmed rotor and OGV. It is depicted with dashed black lines.

3.2 Description of the flow solvers

The 1D meanline calculations (method 1) are conducted with the aerodynamic module integrated in PropNoise [6]. The module is very fast since it takes less than one second to compute the flow properties. This approach focuses on simple and robust analytical models rather than very accurate and extensive models. The steady aerodynamics are calculated at a specified radial position which is considered representative in terms of fan performance. The meanline approach neglects complex radial variations of geometry and flow quantities. Consequently, the rotor blade has a simplified shape, as seen in Fig. 4, and profile param-

eters like profile thickness and stagger angle are given on the meanline position only. The core stream in dual-stream engines is not considered with this method.

The 2D throughflow calculations (method 2) are conducted with the DLR Streamline Curvature Method (SCM) ACDC (Advanced Compressor Design Code) [11]. The computation of the flow field for one operating point takes about two seconds on a single core. For the throughflow setup of the ACAT1 fan, the blades have been re-designed with airfoils from the design system of ACDC. This was done by choosing airfoils that have a similar outflow angle in comparison to a 3D-RANS design-point simulation. Afterwards, the design incidence of the airfoils was adapted to match the fan map. In contrast to the meanline calculations, the ACDC setup includes the split into core and bypass stream. Additional to profile losses, models for spanwise mixing and tip clearance flow are activated in the throughflow code.

The 3D-RANS simulations (method 3) are conducted with the DLR CFD solver TRACE [23]. The computational efforts for this method are very high since it takes about 15 hours on 36 cores to compute the flow field for one operating point. The steady-state simulations are based on the numerical setup by KISSNER et al. [7] with the MENTER SST (Shear Stress Transport) $k-\omega$ turbulence model [24]. Recommended turbulence model extensions supported by TRACE (concerning rotation, transition and the stagnation point) are applied based on a best-practice study detailed in [25] for RANS-informed prediction of fan broadband interaction noise. The fan domain is discretized using a structured multi-block grid with 4.8 million cells. The mesh resolution is particularly high in the interstage region and close to walls because flow characteristics like the rotor wakes and boundary layers are expected in these regions. The blade boundary layers and wakes convected downstream of the rotor need to be carefully resolved for the rotor-stator interaction noise prediction in order to be reliable. For this purpose, the boundary layers on the rotor blade surfaces are fully resolved and the wakes are resolved with approximately 20 cells in azimuthal direction at 75% of the stator height. The domain is split up into a moving rotor block and a steady stator block. These blocks are divided by a mixing plane which circumferentially averages the flow information. A method by JARON [26] extracts the wake and turbulence information at the mixing plane and extrapolates it to the stator leading edge.

3.3 Fan map calculation

For our previous research efforts, the turbulence model for fan-rotor wakes was investigated at a limited amount of operating points. These were usually the noise certification points located on the fan working

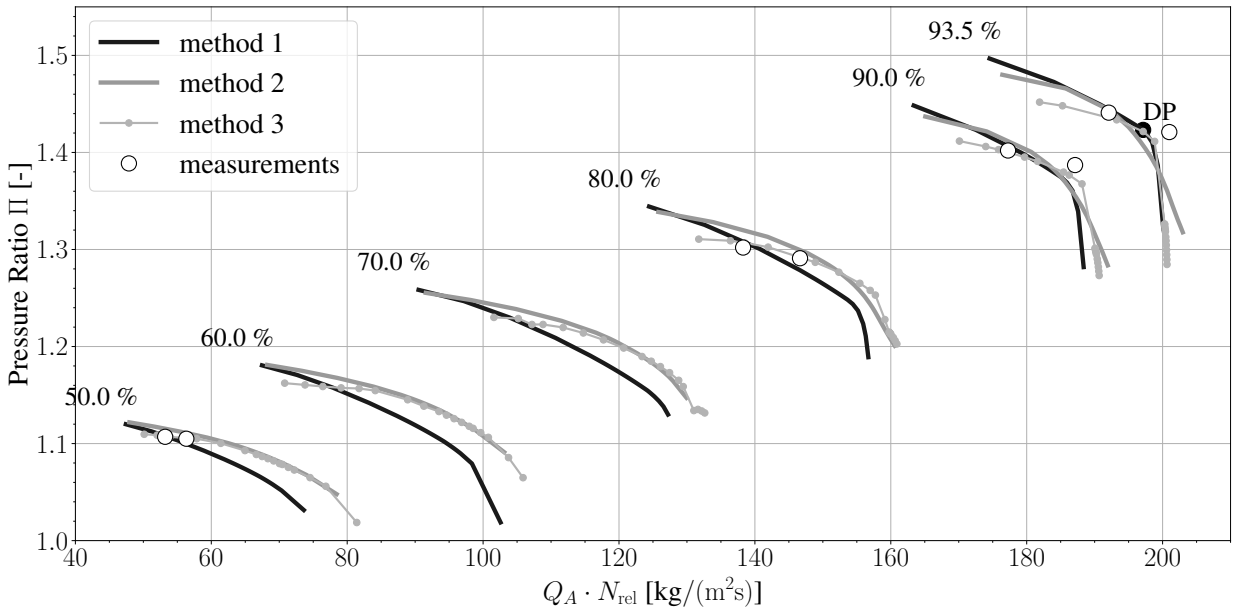

Fig. 5. Pressure ratio over mass flow density fan map calculated with all flow solvers

line. For this paper, the model is studied at a comprehensive number of operating points with a wider range of flow incidences. Thus, six speed lines are calculated as visible in Fig. 5. On each speed line the fan is throttled from surge conditions at lower mass flow rates to choking conditions at higher mass flow rates. The 93.5% design speed line has a fan revolution speed of 7102.6 rpm.

The pressure ratio Π is plotted over the mass flow density $Q_A = \rho W_x$, which is at the same time the ratio of corrected mass flow to cross-section area at the rotor entry plane. Furthermore, in Figs. 5 to 9 and 11 the mass flow rates are multiplied with the relative fan speed $N_{\mathrm{rel}} = N/N100\%$ in order to pull the individual speed lines apart and for the sake of clarity.

4 ANALYSIS AND DISCUSSION

The quantities for the modeling of rotor wakes for broadband noise prediction, as explicated in the *Theory* section, are determined for each operating point shown in Fig. 5. The trends of parameters like rotor losses, wake size, turbulence in the wake and finally acoustic power levels are analyzed and discussed in this section. For this purpose, methods 1 and 2 are opposed to the results from method 3 and microphone measurements. In order to reduce radial distributions to one value for each operating point, the following

diagrams show area averaged values for methods 2 and 3.

4.1 Comparison of estimated mean and turbulent wakes

The ACAT1 fan map shown in Fig. 5 exhibits a good agreement for the pressure ratio between all three methods and measurements. In comparison to method 1 and method 2, a smaller working range especially at higher fan speeds can be achieved with method 3. More complex, three-dimensional flow phenomena are considered in the numerical simulation which leads to earlier flow separation on the rotor blade. In addition, the cold geometry is considered for all fan speeds which results in comparatively high tip clearances at high speed in contrast to reality.

With regard to the mean wake evaluation, the total-pressure loss coefficient and wake area are depicted in Fig. 6. Only a selection of three speed lines are plotted in this diagram for each method for the sake of clarity. Methods 1 and 2 allow a distinction of overall losses (solid) and the viscous part (dashed) which is necessary for the prediction of the boundary layers as described earlier. With method 3, only the overall losses can be deduced from the simulations. The difference between overall and viscous losses are mainly caused by shock-related pressure loss and losses generated by secondary flow in the endwall regions. In general, method 2 seems to predict overestimated losses by an almost constant offset but provides a plausible distinction between viscous and shock losses. Concerning the gradients at high loading, both methods make a sufficient prediction of the loss increase towards the surge margin. On the contrary, the gradients at low loading, that is towards choking conditions, show a good agreement with method 1 at high speeds and a good agreement with method 2 at part speeds. The conservative correction by method 2 of pressures loss for choking at high fan speeds can already be observed in the fan map of Fig. 5. Due to the implemented model, we obtain similar trends when comparing the viscous losses with the wake area as defined in Eq. 4. The increase of wake area close to choking at high speed is not covered by the model since an increase of viscous losses is not expected. Nevertheless, it can be observed for method 3 when strong shocks occur in the fan stage. The width of the wake, as specified in Eq. 5, is not shown here but has been checked. It features similar trends for all three methods compared to the wake area.

Figure 7 depicts the empirical coefficients for the estimation of turbulent quantities as defined in Eqs. 7 and 8. Methods 1 and 2 use constant values. Furthermore, the coefficients are deduced from the flow solution of method 3. With reference to the results from method 3, universal constants for the empirical

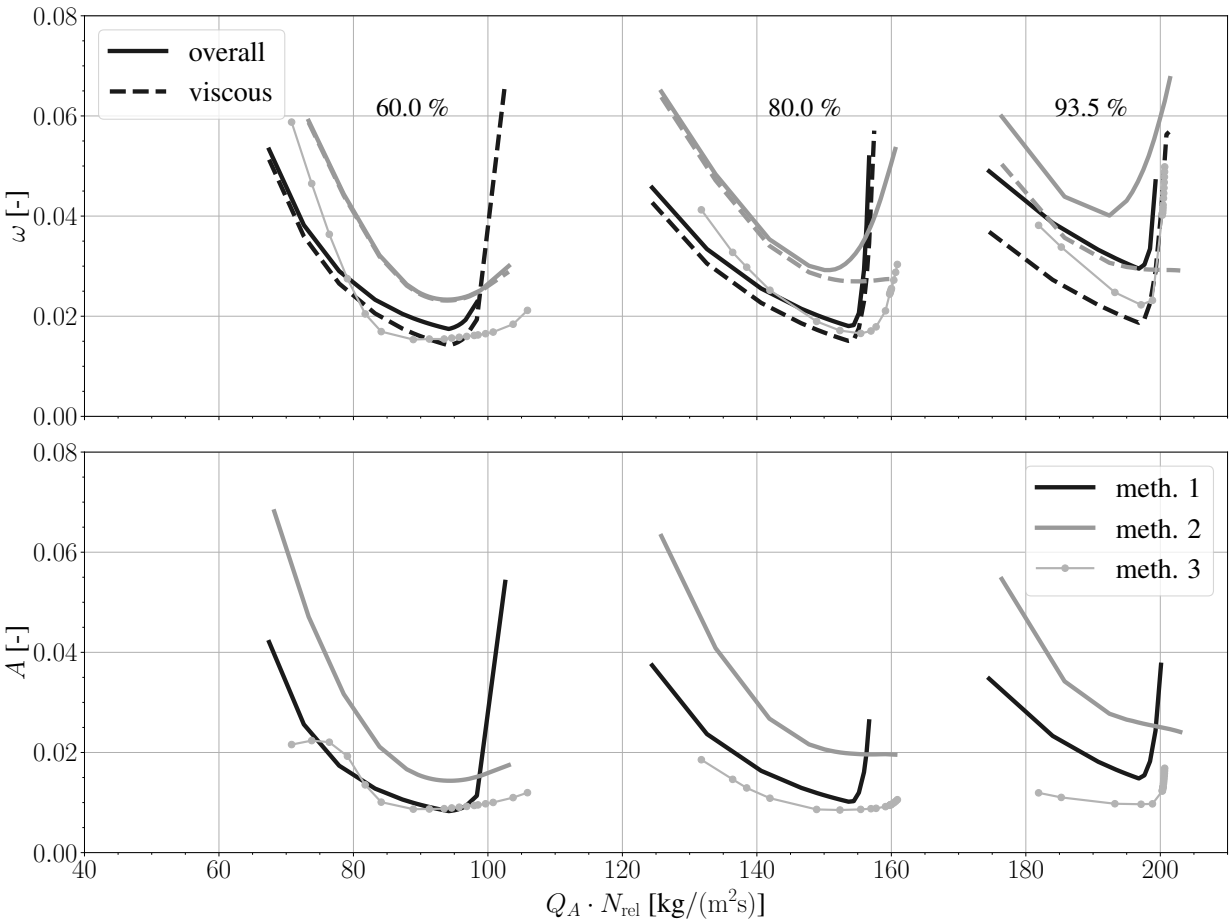

Fig. 6. Pressure loss coefficient (top) and wake area (bottom) over mass flow density

turbulence model seem to be acceptable for a wide range of operating points. The values vary for K_L between 0.25 and 0.4 and for K_U between 0.3 and 0.5. The radial distribution of the empirical coefficients have been assessed for a selection of operating points, too. The radial distribution indicated constant values as well except for the tip region. The influence of the tip region is appraised in the section *Influence of turbulence in tip regions on broadband noise*. In contrast to the constants selected in the previous paper [5], the value of K_U has been reduced from 0.6 to 0.4 which is closer to the values found in the literature. Lower turbulence intensity values compared to the CFD results from the previous paper seem to be responsible for the necessary adjustment. A few possible reasons can be listed to explain the difference in turbulence intensity: On the one hand, the RANS simulations were conducted with an improved meshing for this paper and the inlet turbulence was reduced from 1% to 0.3% in order to match with the measured values during

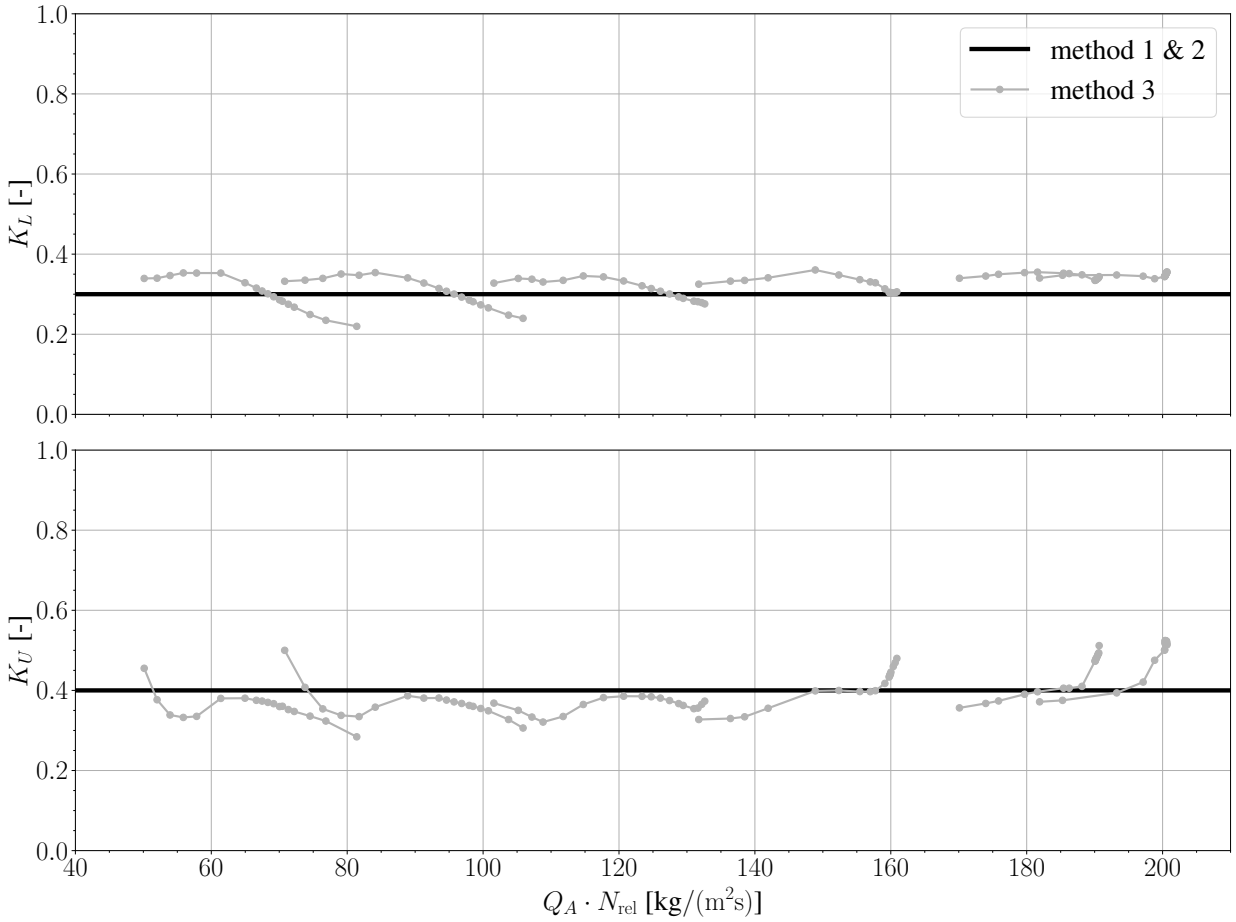

Fig. 7. Empirical coefficients for the estimation of TLS (top) and TKE (bottom)

the experiments. But this should have little effect on wake turbulence as indicated by KISSNER et al. [7]. Except for that, the CFD setups are identical. On the other hand, the method to determine the coefficients differ. In the previous work, the coefficients were calibrated based on the acoustic results whereas in this paper the coefficients are actually calculated based on the evaluated mean wakes and turbulence.

Due to the proportional relationship in the empirical model between mean and turbulent wake, very similar observations as for the loss and mean wake parameters can be made for the normalized turbulent integral length scale L and the turbulent intensity I, when comparing Fig. 6 with Fig. 8. The absolute turbulence values are again overestimated by method 2.

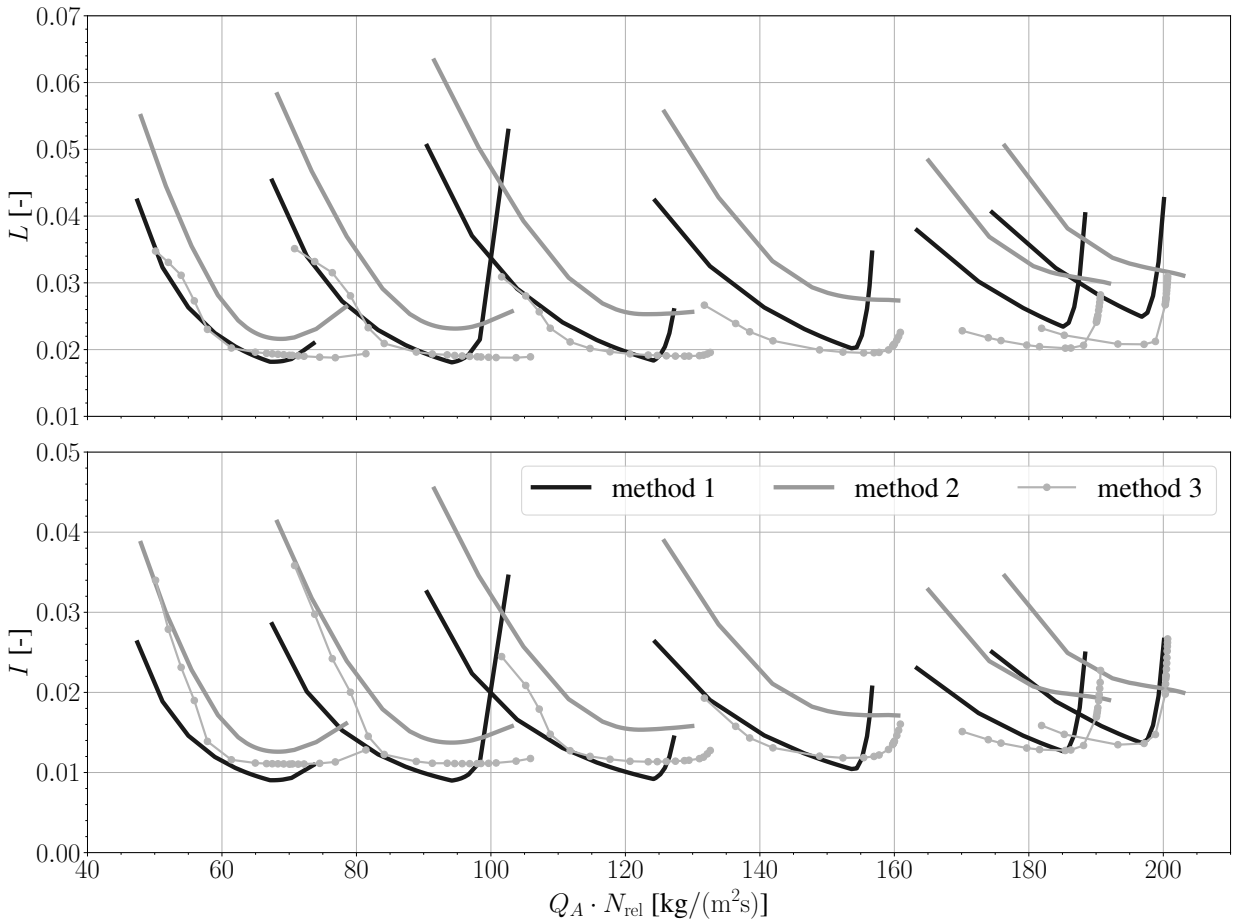

Fig. 8. Normalized turbulent integral length scale (top) and turbulent intensity (bottom) over mass flow density

4.2 Broadband rotor-stator wake interaction noise prediction

After reviewing the predicted aerodynamic quantities, like pressure loss, mean wake size and wake turbulence, in the previous section, their influence on the broadband RSI noise is analyzed and discussed in this section. The resulting overall sound power levels PWL$= 10\log_{10}(P/10^{-12})$ based on the different flow solutions are plotted in Fig. 9. The noise source is transmitted upstream (top) and downstream (bottom) into the far-field and compared to the microphone measurements.

So far, no acoustic shielding is implemented into the analytical noise prediction tool. This explains why the predicted noise levels continuously increase with increasing fan speed while the measured upstream sound power levels decrease starting from 80% fan speed. When comparing the RANS-informed reference method with the experimental data, we observe a good agreement concerning the gradients PWL over flow

incidence but the absolute PWL are below the measured PWL. This is an expected result because numerous noise sources are measured during the experiments whereas only one noise source is investigated with the presented methods. Especially at low frequencies, spurious measured noise can be observed and trailing edge noise is supposed to be another important contributor to broadband fan noise.

Apart from that, similar statements about the fan map trends can be made as in the preceding section about the aerodynamic quantities. Method 2 suddenly shows a good agreement of absolute values compared to the results from method 3. In general, three questions arise when comparing the results from the turbulence quantities seen in Fig. 8 with the noise results seen in Fig. 9:

1. Why do the noise levels predicted by method 3 increase for low loading at part speed even though TKE and TLS remain almost constant?
2. Why do the noise levels predicted by method 3 increase with increasing fan speed along a working line even though TKE and TLS remain almost constant?
3. Why are the noise levels mostly aligned for methods 2 and 3 even though method 2 overestimates TKE and TLS compared to method 3?

In order to find answers to all three questions, it is necessary to keep in mind that not only the turbulence in the fan-rotor wakes contributes to broadband noise but also the flow velocity of the wakes impinging on the OGV has a non-negligible influence. A very simple way to estimate acoustic power trends can be undertaken with the acoustic scaling law, which can be defined for the broadband wake interaction noise as $P \propto W^{3\sim4} \cdot \mathrm{TKE}$. The formula suggests a strong dependency to the flow velocity at the stator leading edge with a power of three or four. Plotting the scaling law over mass flow density shows very similar trends as predicted by the analytical noise prediction approach.

4.3 Influence of turbulence in tip regions on broadband noise

To estimate the influence of flow phenomena like tip leakage or endwall boundary layers in the tip region of the OGV on the interaction broadband noise source, the turbulence parameters TLS and TKE are synthetically clipped in this part of the radial distribution. That is, the value of TLS and TKE calculated with the RANS simulation at 90% relative rotor height is kept constant for the last 10% and the usually steep slope is removed as if the flow is unaffected by the casing and rotor tip clearance. A comparison

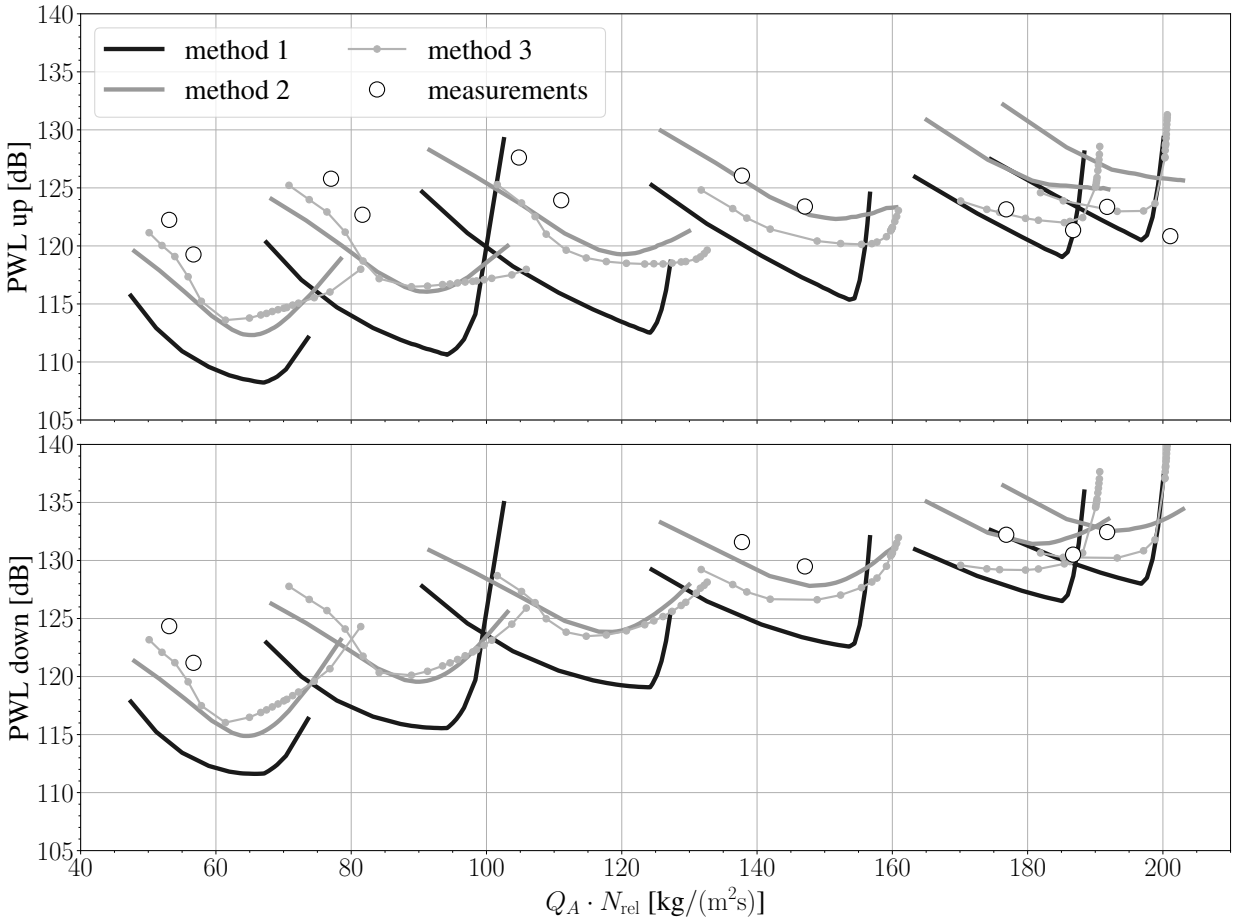

Fig. 9. Overall sound power levels for broadband rotor-stator wake interaction noise in upstream (top) and downstream (bottom) direction

of the broadband noise results *with clipping* and *without clipping* is supposed to give an estimation of the contribution of turbulence in the tip region on the noise prediction by the applied method.

Figure 10 depicts the radial distribution of an exemplary operating point at approach speed for the normalized TLS L (left) and the turbulent intensity I (right). The turbulent intensity is not exactly constant because it also depends on the radial distribution of flow velocity. The selected turbulence model in the RANS simulation describes a decrease of TLS and an increase of TKE in the tip region. Since both parameters influence the amplitude of the VON KÁRMÁN spectrum, it can be assumed that they could cancel each other's influence on broadband noise.

This clipping procedure is applied to all flow solutions of the numerical CFD simulation and the influence of turbulence in the tip region on broadband noise is once again evaluated for all operating points of

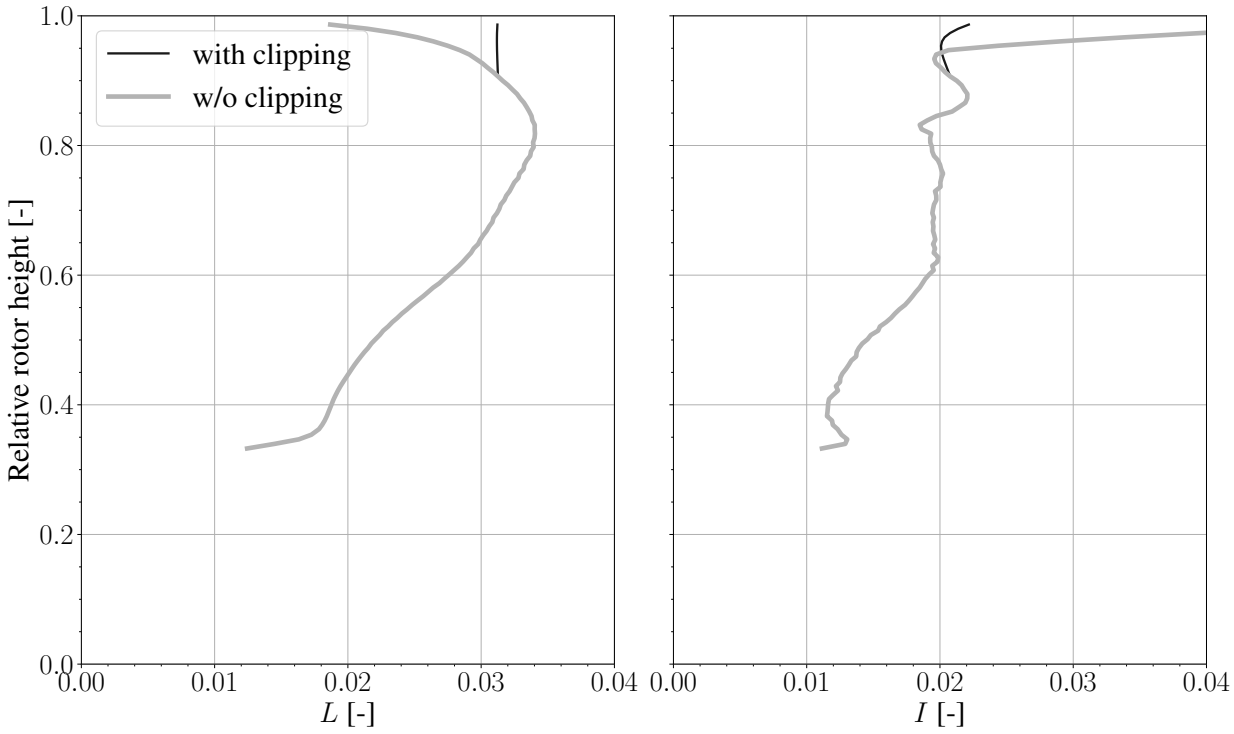

Fig. 10. Radial distribution of normalized TLS (left) and turbulent intensity (right) at approach condition

the presented fan map. Figure 11 shows the exemplary 50% speed line only since the difference between the resulting speed lines are very small. The maximum delta between clipped and non-clipped calculations are around 0.5 to 1 dB. It is noteworthy that the results show an almost constant offset between the calculations and that the deltas do not increase much for increasing incidence angles. When regarding method 3 as the reference, it can therefore be concluded that method 1 and method 2, which do not consider complex 3D flow structures, seem to be justified for broadband noise prediction during preliminary design. Those methods should still provide sufficiently correct trends even at off-design operation during this early phase of fan design.

5 CONCLUSION

The purpose of this paper was to study the applicability of a meanline and a throughflow method to provide aerodynamic parameters for analytical fan broadband noise prediction. An empirical model is utilized for both approaches to translate the steady aerodynamic parameters (total-pressure loss of the fan-rotor) into

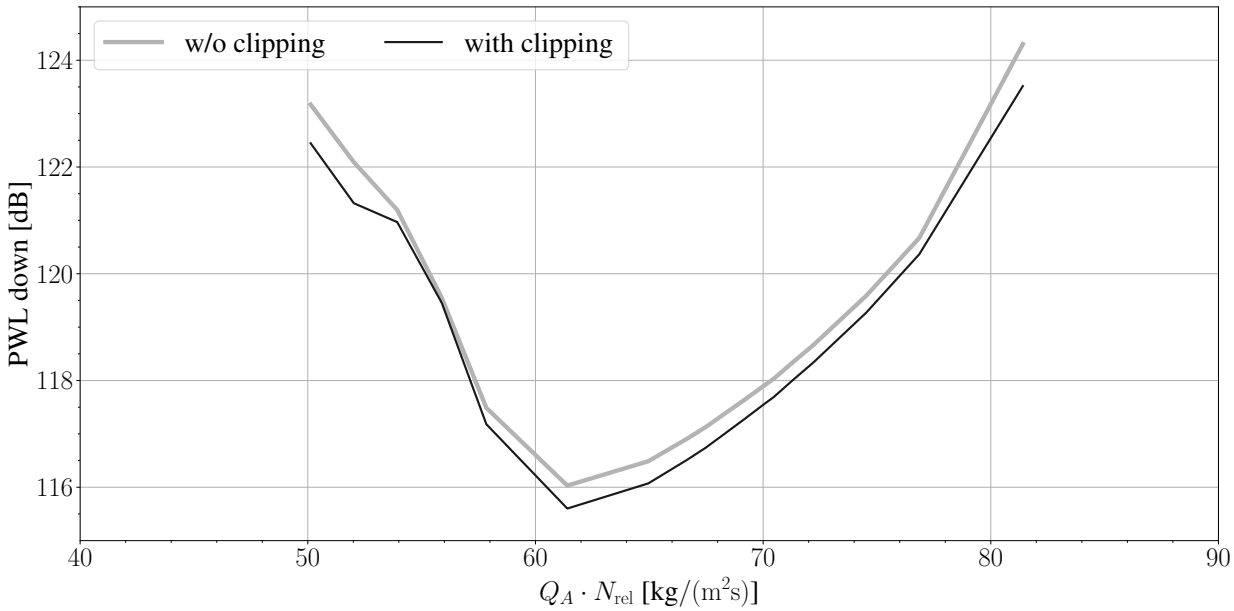

Fig. 11. Overall sound power levels for 50% speed line over mass flow density

unsteady aerodynamic parameters (mean and turbulent wake). Reference data was provided by a RANS-informed analytical noise prediction method and microphone measurements. By this means, the findings of a previously published paper were extended and reviewed. In contrast to the previous publication, this paper focuses on a broad working range of a fan stage, a comparison of mean wake profiles in circumferential direction and a more precise RANS-based determination of the empirical coefficients for the turbulence model.

Method 1, which calculates the flow on a representative mean streamline, shows an overall good prediction of loss, mean wake, turbulent wake and broadband PWL trends. The average difference of PWL for all operating points is about ΔPWL=-4 dB compared to method 3. The approach overestimates losses when shocks are expected to occur at part speed. A new aerodynamic model, which is better suited for thin supersonic fan blades, has already been developed and will be implemented soon. It is supposed to provide a better distinction of viscous and shock loss.

Method 2, which calculates the flow on several streamlines, exhibits an overall very good prediction of broadband PWL in terms of absolute values and the trends of loss, mean wake and turbulent wake. The average difference of noise prediction to method 3 is ΔPWL=+0.5 dB. The approach overestimates the

absolute values of total-pressure loss and underestimates the increase of loss for choking at high speed.

Method 3, which calculates a 3D representation of the flow field, seems to be a valid reference method when comparing the broadband PWL trends to measurements and considering evaluated applications found in the literature.

All three methods indicate one operating point for each speed line that exhibits minimum losses, small wakes and little turbulence as well as low broadband noise levels. This point is usually the operating condition with low incidence, that is with favorable rotor inflow conditions. For conventional fan stages these conditions are only maintained for the cruise flight operation. But variable geometries like a variable-area nozzle (VAN) or a variable blade pitch can help to meet these conditions for different fan speeds and therefore improve fan aerodynamics and acoustics at the same time. MOREAU [27] studied the theoretical acoustic benefit of VANs. This study concludes that the application of a VAN can slightly increase fan tonal noise whereas fan broadband noise is reduced by more than 5 dB and jet noise by 2-3 dB.

The results confirm the validity of the assumption that wake turbulence scales proportionally with the mean wake. The coefficients of proportionality are weak functions of the radial position, the operating conditions and the fan configuration considered. Due to the increased turbulence production in the endwall regions of a fan stage, the results indicate an exception from the assumption in this region. But the contribution of turbulence close to endwalls seems to be negligible for wake interaction broadband noise prediction because the average contribution is estimated with ΔPWL=+0.4 dB only.

In conclusion, it can be stated that the methods 1 and 2 as well as the empirical turbulence model seem to be appropriate methods for broadband noise prediction during the preliminary design phase - also when calculating operating points aside the usual operating range of a fan stage. For prospective studies it should be considered to check the mean wake and turbulence parameters with hot-wire measurements. Additionally, an appraisal of the contribution of background turbulence to broadband noise is recommended. Furthermore, it is also possible to estimate the tonal part of the RSI noise with the analytical noise prediction tool PropNoise. Hence, an investigation of the influence of mean wakes on tonal noise is planned next.

ACKNOWLEDGEMENTS

The presented work was funded by the German Federal Ministry for Economic Affairs and Climate Action, as part of the LuFo VI research project MUTE under grant agreement No. 20T1915D.

The numerical and experimental investigations on the ACAT1 fan stage were conducted in the frame of the project TurboNoiseBB, which has received funding from the European Union's Horizon 2020 research and innovation program under grant agreement No. 690714. The authors are grateful for the numerical setup and meshing provided by Dr. Carolin Kissner.

The authors also want to thank their colleagues from the Engine Department (DLR Institute of Propulsion Technology) for the technical support concerning the interface between ACDC and PropNoise.

REFERENCES

[1] Moreau, S., 2018, "Turbomachinery-related aeroacoustic modelling and simulation," In Proceedings of 17th International Conference on Fluid Flow Technologies, pp. 4–7.

[2] Moreau, S., 2019, "Turbomachinery Noise Predictions: Present and Future," *Acoustics,* **1**(1), Jan., pp. 92–116.

[3] Moreau, S., and Roger, M., 2018, "Advanced noise modeling for future propulsion systems," *International Journal of Aeroacoustics,* **17**(6-8), July, pp. 576–599.

[4] Peake, N., and Parry, A. B., 2012, "Modern Challenges Facing Turbomachinery Aeroacoustics," *Annual Review of Fluid Mechanics,* **44**(1), Jan., pp. 227–248.

[5] Meier zu Ummeln, R., and Moreau, A., 2020, "Estimation of turbulence in fan-rotor wakes for broadband noise prediction during acoustic preliminary design," In AIAA AVIATION 2020 FORUM, American Institute of Aeronautics and Astronautics.

[6] Moreau, A., 2016, "A unified analytical approach for the acoustic conceptual design of fans of modern aero-engines," Doctoral Thesis, Technische Universität Berlin, Berlin, July.

[7] Kissner, C., Guérin, S., Seeler, P., Billson, M., Chaitanya, P., Carrasco Laraña, P., de Laborderie, H., François, B., Lefarth, K., Lewis, D., Montero Villar, G., and Nodé-Langlois, T., 2020, "ACAT1 Benchmark of RANS-Informed Analytical Methods for Fan Broadband Noise Prediction—Part I—Influence of the RANS Simulation," *Acoustics,* **2**(3), July, pp. 539–578.

[8] Guérin, S., Kissner, C., Seeler, P., Blázquez, R., Carrasco Laraña, P., de Laborderie, H., Lewis, D., Chaitanya, P., Polacsek, C., and Thisse, J., 2020, "ACAT1 Benchmark of RANS-Informed Analytical Methods for Fan Broadband Noise Prediction: Part II—Influence of the Acoustic Models," *Acoustics,* **2**(3), Aug., pp. 617–649.

[9] Lewis, D., Moreau, S., Jacob, M. C., and Sanjosé, M., 2021, "ACAT1 Fan Stage Broadband Noise Prediction Using Large-Eddy Simulation and Analytical Models," *AIAA Journal*, July, pp. 1–21.

[10] Drela, M., and Youngren, H., 1998, *A User's Guide to MISES 2.53* MIT Aerospace Computational Design Laboratory, Cambridge, MA, United States.

[11] Schnös, M., 2020, "Eine Auslegungsmethodik für mehrstufige Axialverdichter auf Basis einer Profildatenbank," Doctoral Thesis, Ruhr-Universität Bochum, Bochum, Aug.

[12] Grieb, H., 2009, *Verdichter für Turbo-Flugtriebwerke* Springer, Berlin Heidelberg, Germany.

[13] Lieblein, S., 1957, Analysis of experimental low-speed loss and stall characteristics of two-dimensional compressor blade cascades Tech. Rep. NACA-RM-E57A28, National Advisory Committee for Aeronautics. Lewis Flight Propulsion Lab., Cleveland, OH, United States.

[14] König, W. M., Hennecke, D., and Fottner, L., 1996, "Improved Blade Profile Loss and Deviation Angle Models for Advanced Transonic Compressor Bladings: Part I—A Model for Subsonic Flow," *ASME J. Turbomach,* **118**(1).

[15] Roger, M., 1994, "Sur l'utilisation d'un modèle de sillages pour le calcul du bruit d'interaction Rotor-Stator," *Acustica,* **80**(3), May, pp. 238–246.

[16] Pope, S. B., 2000, *Turbulent flows* Cambridge University Press, Cambridge, New York, USA, Aug.

[17] Jurdic, V., Joseph, P., and Antoni, J., 2009, "Investigation of rotor wake turbulence through cyclostationary spectral analysis," *AIAA Journal,* **47**(9), Sept., pp. 2022–2030.

[18] Ganz, U. W., Joppa, P. D., Patten, T. J., and Scharpf, D. F., 1998, Boeing 18-inch fan rig broadband noise test Technical Report NASA/CR-1998-208704, Boeing Commercial Airplane Group, Hampton, Virginia, USA, Sept.

[19] Wygnanski, I., Champagne, F., and Marasli, B., 1986, "On the large-scale structures in two-dimensional, small-deficit, turbulent wakes," *Journal of Fluid Mechanics,* **168**, July, pp. 31–47.

[20] Behn, M., and Tapken, U., 2019, "Investigation of Sound Generation and Transmission Ef-

fects Through the ACAT1 Fan Stage using Compressed Sensing-based Mode Analysis," In 25th AIAA/CEAS Aeroacoustics Conference, American Institute of Aeronautics and Astronautics.

[21] Tapken, U., Behn, M., Spitalny, M., and Pardowitz, B., 2019, "Radial mode breakdown of the ACAT1 fan broadband noise generation in the bypass duct using a sparse sensor array," In 25th AIAA/CEAS Aeroacoustics Conference, American Institute of Aeronautics and Astronautics.

[22] Tapken, U., Pardowitz, B., and Behn, M., 2017, "Radial mode analysis of fan broadband noise," In 23rd AIAA/CEAS Aeroacoustics Conference, American Institute of Aeronautics and Astronautics.

[23] Becker, K., Heitkamp, K., and Kugeler, E., 2010, "Recent Progress In A Hybrid-Grid CFD Solver For Turbomachinery Flows," In Proceedings of the V European Conference on Computational Fluid Dynamics ECCOMAS CFD 2010.

[24] Menter, F. R., 1994, "Two-equation eddy-viscosity turbulence models for engineering applications," *AIAA Journal,* **32**(8), Jan., pp. 1598–1605.

[25] Jaron, R., Herthum, H., Franke, M., Moreau, A., and Guérin, S., 2017, "Impact of turbulence models on RANS-informed prediction of fan broadband interaction noise," In European Conference on Turbomachinery Fluid Dynamics and hermodynamics.

[26] Jaron, R., 2018, "Aeroakustische Auslegung von Triebwerksfans mittels multidisziplinärer Optimierungen," Doctoral Thesis, Technische Universität Berlin, Berlin, May.

[27] Moreau, A., 2021, "Theoretical acoustic benefit of high bypass ratio and variable-area nozzle in turbofan engines," In Proceedings of the 14th European Conference on Turbomachinery Fluid Dynamics and Thermodynamics.